An Exploration of Stochastic Fatigue Effects of Micro-cracks in Polymer Composites

Alison J McMillan

Rolls-Royce plc

Abstract: There is increasing interest in the use of organic matrix composite materials in aerospace, as it is commonly stated that composite materials show good fatigue properties. This is rather difficult to quantify. Fatigue testing to obtain a S/N curve or a Range-Mean diagram for a composite material is fraught with difficulties; test specimens are prone to significant manufacture variation and it is time consuming to get data for high fatigue life. It is recognized that micro-cracks exist in composite components that would normally be considered "undamaged". It has also been found that such cracks show evidence of crack growth during fatigue testing, although such growth is tiny in the length scale of the component. With sufficient numbers of micro-cracks, the effect of crack interaction is anticipated where each crack tip stress intensity factor is higher than it would be in a single crack in isolation. Thus, the fatigue of a composite specimen may show several phases; (i) initially no macroscopic damage, (ii) rapid increase in the micro-crack growth as crack interaction becomes significant, macroscopically this might show in reduced residual component strength, (iii) micro-cracks begin to coalesce, grow much more rapidly and become macroscopic cracks. The objective of this work is to use Abaqus, in conjunction with iSight and XFEM to make micro-scale models of regions of composite material containing micro-cracks. Sizes and densities of micro-cracks will be varied in order to determine the changes of behaviors (i-iii) above, and identify any other phenomenological behavior to investigate in future experimental work.

Keywords: Boundary Conditions, Composites, Crack Propagation, Damage, Delamination, Failure, Fatigue, Fatigue Life, Fracture, Representative Volume Elements.

1. Introduction

The motivation for this piece of work is the observation that composite materials do not have well defined fatigue characteristics. Fatigue testing of composite specimens generally yields results with a high scatter, and there are difficulties associated with testing at high life. Furthermore, just as there are different stiffness characteristics in a composite, governed by the directionality of its layup and the load application direction, there are also differences in fatigue strength. As a result, to generate an appropriate set of S/N curves for a composite material is expensive in the number of tests required and still leaves a great deal of uncertainty, particular in terms of the fatigue strength characteristics of materials at high life. There is a school of thought that at sufficiently low levels of cyclic load, there will be no crack growth, but fatigue testing beyond around 10^7 cycles is not practical.

The difficulty arises because of the way that the concepts of fatigue have been developed, alongside the development of the 20th century engineering materials: *i.e.* metals. Metals are reasonably homogeneous at the macroscopic length scale; that is, at the length scale of the engineering component, or the length scale that FEA is generally performed. The composite materials considered here are comprised of fibers or glass or carbon embedded in an organic matrix.

To achieve the required engineering requirements of a component, the fibers must be orientated to provide the requisite strength and stiffness in the load bearing directions, and a material layup created to fill the necessary volume. For complex components, fibers will not generally take a straight path, there may be ply-drops to accommodate thickness changes, and there may even be through-thickness reinforcement fibers. As a result, the resin volume fractions will vary throughout the component, and there may also be significant resin pockets (Gerlach, to appear).

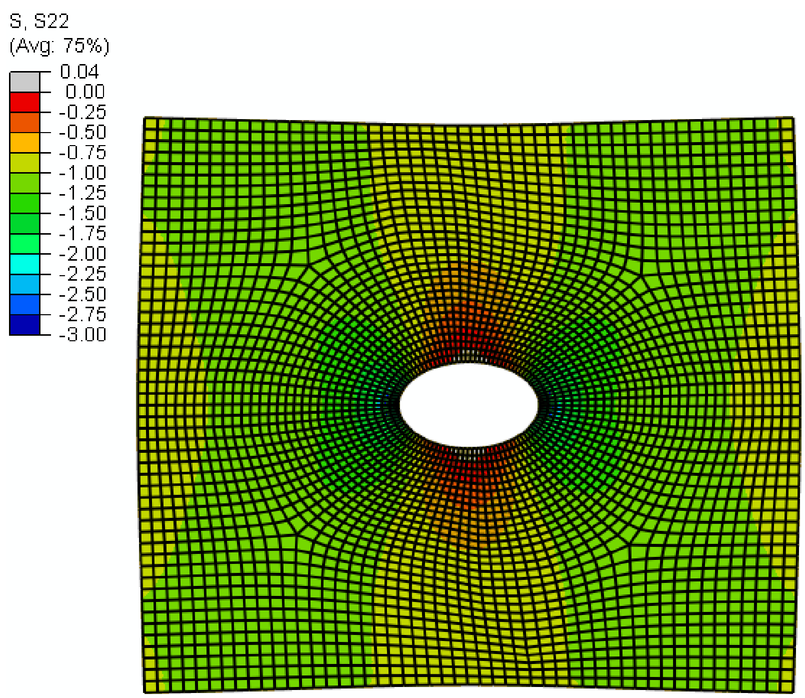

Figure 1. Case study under pressure loading and 3DOF BCs.

2. Approaches to random crack modeling

The research presented here sets out to model composites at the resin pocket length scale. It acknowledges that the resin pockets are low strength regions in a highly constrained stress field, and seeks to understand the effects on the stress field of randomly positioned flaws or cracks in the resin at microscopic scales. The ultimate objective is to determine at which size or concentration of micro-cracks the stress intensity becomes great enough to initiate crack growth, not simply extension of each micro-crack in isolation, but the general merger of many such cracks to give rise to a macroscopic effect.

This approach, although straight forward for those familiar with finite element techniques, opens a number of questions in other areas of mathematical modeling, particularly statistics. For example, Wilson and Taylor (1997) take a Monte Carlo Markov Chain approach to model the crack propagation phases of micro-cracks in a molybdenum alloy. Regards practical methods of assessing crack density in a test specimen or component, there is little to be found, but methods used for estimation of quantities of wood lying on the ground (Van Wagner, 1982), or for estimating the amount of root in a quantity of soil (Newman, 1966), may be adapted.

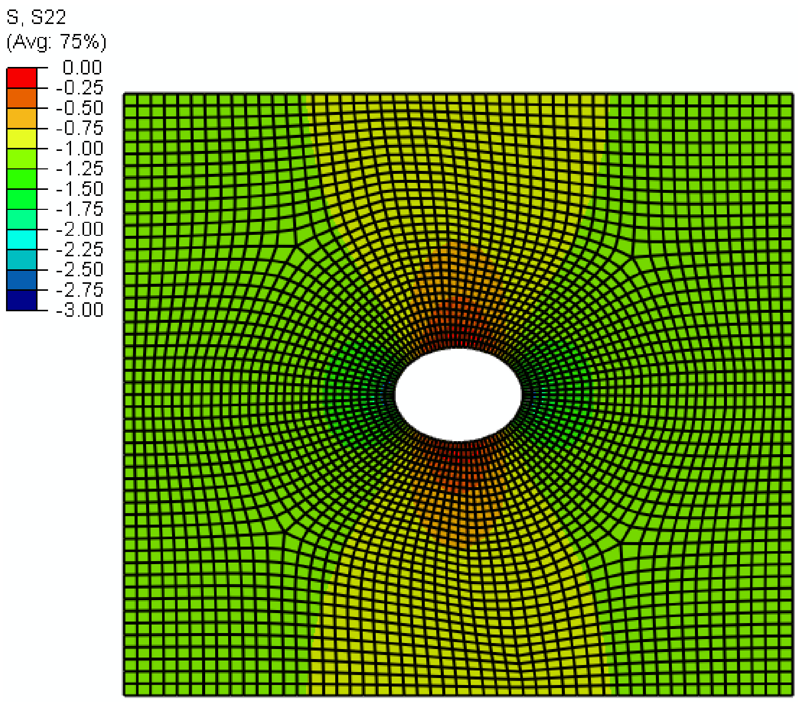

Figure 2. Case study under pressure loading and RVE BCs.

3. Modeling Issues

Given the nature of the research, some care needs to be taken to ensure that the modeling is as effective as it can be. As this is to be the first step in a stochastic study, the efficiency of pre-processing, analysis and post-processing are major considerations.

Firstly, it is necessary to choose a simple problem domain; a RVE (representative volume element). The RVE approach usually assumes real symmetry between the RVE and its neighbors, and requires application of boundary conditions in respect of this. It might be reasonable to select a volume of material, and make the assumption that all neighboring material is of similar stuff and subject to similar stress fields. In reality, resin pockets are small, and bounded by fibers. The Young's modulus of fiber material in its longitudinal direction is between 10 and 100 times that of the resin, so it is clear that proximity to fibers would have a significant influence on the stress state of the resin.

A second issue is to consider the modeling of the micro-cracks. The flaws to be found in the resin may be voids or inclusions, having a rounded boundary, or they may be line cracks. It is well known that if a crack is represented as having a point tip, then the stress at the tip is undetermined. The alternative is to represent the cracks by a shape such as an ellipse. Even so, for a small curved feature, the anticipated Stress Intensity Factor (SIF) is high, and the nature of FEA is to under-predict compared with theory (Pilkey, 1997), even for very high mesh densities.

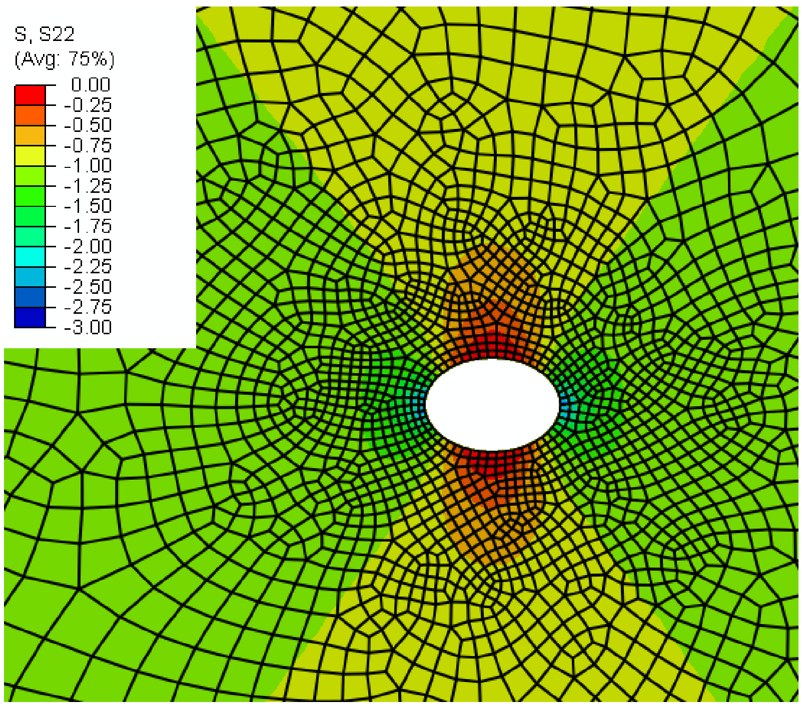

Figure 3. Case study of ten times the size and RVE BCs.

3.1 Simple test case

Before launching into modeling complex patterns of micro-cracks, a simple test case was devised. It was decided to limit the modeling to 2D plane strain. In view of the micro-scale sizes adopted, all Abaqus modeling was performed with units of mm and MPa.

The basic geometry was a square of resin, side length 5µm, with a central circular hole of diameter 1µm. The resin Young's modulus was taken to be 2890 MPa (HEXCEL, HexFlow® RTM 6 data), Poisson's ratio 0.3.

A number of combinations of load case and boundary condition were tried, with a view to establishing which was easiest to apply and maintained symmetry appropriately for a RVE.

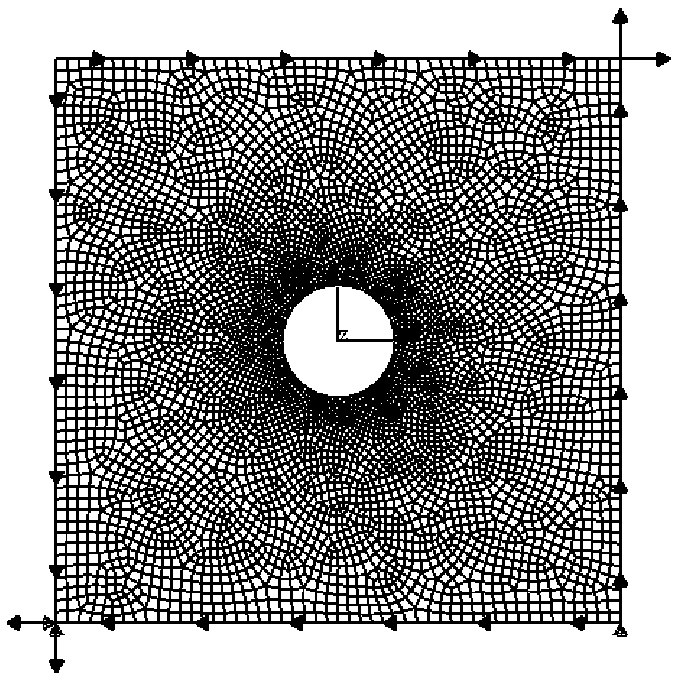

Figure 4. Mesh, shear loads and BCs for simple case study.

3.2 Adequacy of FE for Stress Intensity Factor calculation

The theoretical value for the SIF at the edge of a circular hole in a uniform uni-axial stress field is three. This was found hard to replicate using FEA. Values approaching three could be achieved by applying a uniform pressure load to both top and bottom of the square, and applying only the minimum 3 DOF boundary conditions. A better approximation could be achieved by increasing the mesh resolution around the hole, see figure 1.

It is worth noting that the above load and boundary condition set up is not consistent with a RVE approach. Figure 1 clearly shows the distortion of the external boundary. Given the symmetries imposed by such boundaries, the RVE model is equivalent to modeling an infinite sheet with regularly spaced holes (Bailey and Hicks, 1960). By applying appropriate RVE boundary conditions, as shown in figure 2, the SIF prediction is around 20% lower.

A further question is the effect of the relative size of the RVE and the hole. A new geometry was created, with ten times the dimensions, and RVE boundary conditions applied (figure 3). Even in this case, and with a highly refined mesh, the SIF was 5-10% below the single hole in a uniform stress field case.

In view of the facts that (i) high mesh resolution is computationally expensive, and (ii) that with the uncertain boundary conditions and the presence of multiple cracks, a uniform stress field is a long way from reality, a more pragmatic approach must be taken to defining what would be an "adequate" quality for a model. The approach taken here was:

1. Choose a mesh seed size, and use this in all models
2. Choose a standard RVE size, and use this in all models
3. Be pragmatic about boundary conditions

3.3 Shear load case and results

The easiest load case to prescribe was found to be that of pure shear, where each side of the square was given a uniform surface traction load of 1.0 MPa, along with the minimum 3 DOF boundary conditions, see figure 4.

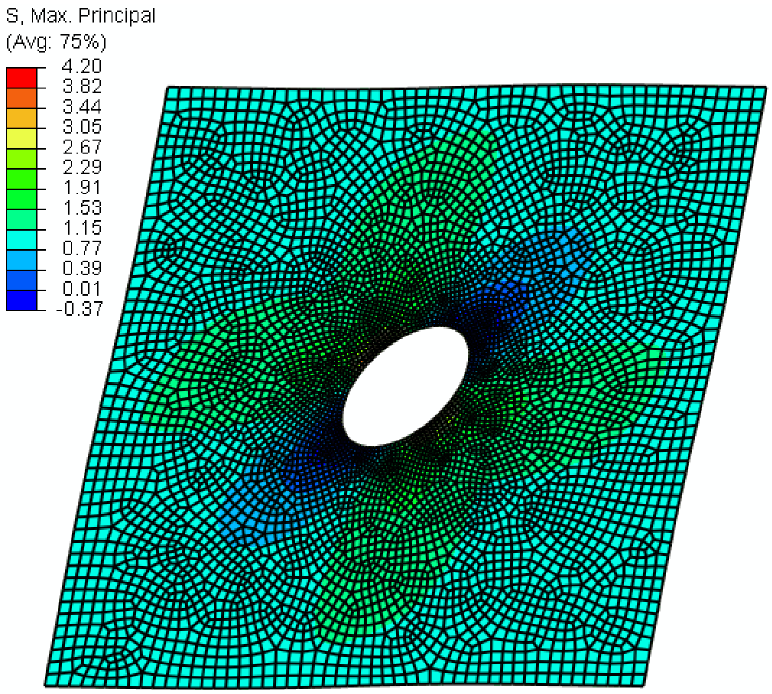

Figure 5. Maximum principal stress plot of test case under applied shear.

A further consideration indicating in favor of a shear load test case is that the loading applied in a resin pocket or between layers of a laminate is predominantly shear. The neighboring fibers, being relatively stiff compared with the resin, will tend to apply surface traction loads.

No specific boundary conditions or constraints were applied to the sides of the domain, as this would have over-constrained it. It is possible to see, in figure 5, that under shear deformation, the sides do not remain straight. In this case, it is clear enough that the distortion shows rotational symmetry and thus the deformed shape would tessellate, and therefore would fulfill the requirement of a RVE. Ultimately, the aim is to represent a number of randomly placed cracks on a single domain, and inevitably this will lead to distortions that are very irregular. Even in that context, the effect of applied shear is not to change volume.

Figure 6 shows an enlarged view of the maximum principal stresses, plotted to the same contour scale as given in figure 5. The hole is shown as elliptical, as this is an exaggerated deformation plot. The highest tensile stress is found on the 45° diagonal intersecting the top left and bottom right of the hole, and would tend to open cracks leading from these points in opposing directions along this diagonal.

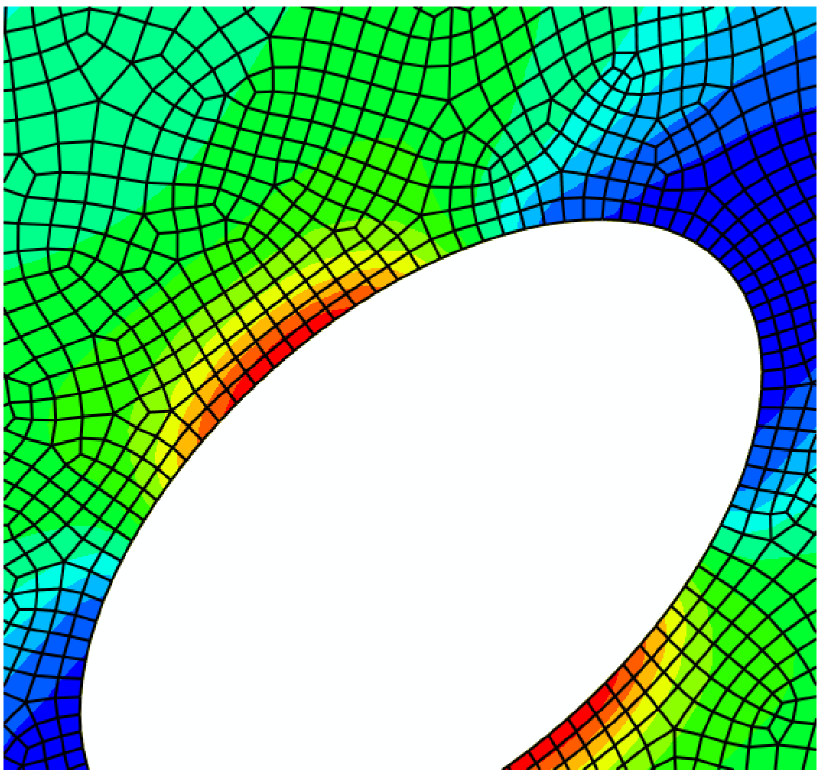

Figure 6. Close-up view of maximum principal stress at hole edge.

4. Computational experiments – Modeling

It was decided to use a RVE approach to modeling, with various distributions of cracks located within the RVE. The RVE would be subjected to applied surface traction loads, as in the shear test case described in section 3.

In the present study, the locations of the micro-cracks are considered random, and a stochastic approach is used to place the cracks within the RVE. Inevitably this means that some cracks will intersect, particularly as the number of cracks increases. A choice also had to be made: whether to allow cracks to cross the edge of the boundary, or to retain a margin of undamaged material around the circumference of the domain. The benefit of the latter would be a reduced influence of inadequacy of boundary effects, and a somewhat simpler approach to applying the surface traction loads. The argument against, is that the margin area would be unrepresentative of real material.

In the present case study, the dimensions of domain and crack were chosen practically such that there would be a maximum of around 10-20 cracks before there was a high probability of cracks interpenetrating sufficiently to disconnect regions of the domain. The number was chosen to be large enough to give some interesting insights, but small enough to be managed by interactive use of Abaqus-CAE. (Automation of geometry definition, meshing and analysis will follow in later investigations.) At such a domain size, a defined margin without cracks was felt to be too great a fraction of the overall domain. In view of this, it was decided to allow cracks to be defined at any point on the domain.

Table 1. Ellipses generated for case study.

Co-ords of centre		Angle (degrees)	Status
x	y		
-1.61E-03	2.93E-03	138	Reject
1.20E-03	1.37E-03	3	Crack 1
-1.12E-03	1.3E-04	43	Crack 2
-1.41E-05	-1.68E-03	31	Crack 3
-2.00E-03	6.7E-04	86	Crack 4
4.6E-04	-2.96E-03	146	Reject
2.45E-03	-8.3E-04	33	Crack 5
2.30E-03	1.82E-05	40	Crack 6
2.34E-03	-1.4E-04	6	Crack 7
1.28E-03	-2.81E-03	43	Clips boundary
1.84E-03	2.92E-03	128	Reject
2.51E-03	3.6E-04	37	Clips boundary
-5.9E-04	1.55E-03	37	Crack 8
5.0E-04	-1.76E-03	10	Crack 9
3.1E-04	-1.40E-03	70	Crack 10
2.36E-03	-2.88E-03	48	Reject
-2.28E-03	9.8E-04	66	Crack 11
-7.1E-04	-2.46E-03	157	Crack 12

4.1 Model geometry

The domain size was chosen as being a square of side length 5μm, with loading and boundary conditions as shown in figure 4.

To simplify the modeling, the cracks were chosen to be ellipses of uniform size; length 1μm, and breadth 0.2μm. The location and orientation of each crack were specified using three random numbers. The random numbers were generated using the RAND() function in MSExcel2007. The first two numbers defined the center coordinates of the ellipse, and the third its orientation with respect to the horizontal. Co-ordinates were rounded to the nearest 0.01μm, and angles to the nearest degree.

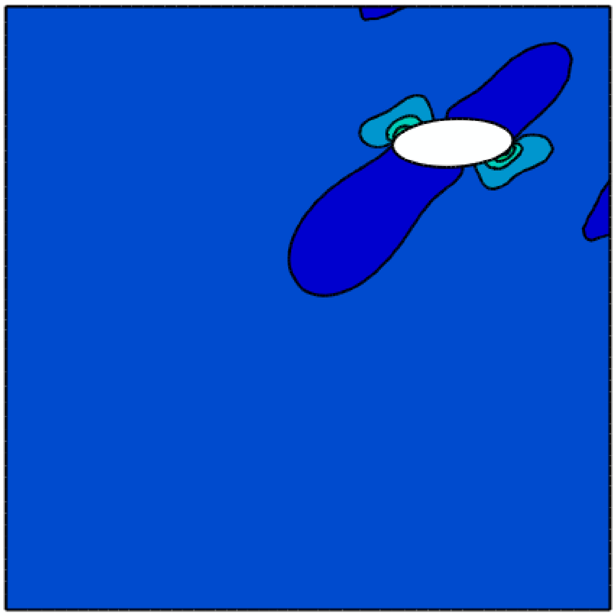

Figure 7. Maximum principal stress – test case with 1 holes.

4.2 Modeling principals

Care was taken to allow the ellipse centers to fall anywhere such that a part of the ellipse could potentially cut the model domain. In practice, given the ellipse orientation, many ellipses with centers within a major half axis distance of the boundary did not in fact intersect the domain. Rather than determine geometrically which ellipses to reject, it was easier to model them within Abaqus-CAE, and test for intersection there.

For the unbroken boundaries, the surface traction was defined with magnitude of 1. Where ellipses intersected with a boundary, clearly there could be no surface traction applied over the region of the intersection. In order to balance the traction loads, it was necessary to calculate the reduction in unbroken edge length, and scale up the applied surface traction proportionately.

As a matter of principal, ellipses with centers within the domain counted towards the "number" of cracks within the domain, irrespective of whether or not they were wholly located within the domain. To balance this, ellipses that had centers outside the domain, but clipped the edge of the domain, were added to the model in the sequence that they were defined, but did not count towards the "number" of cracks. The co-ordinates, orientations and the status of each ellipse generated for use in this case study are given in table 1.

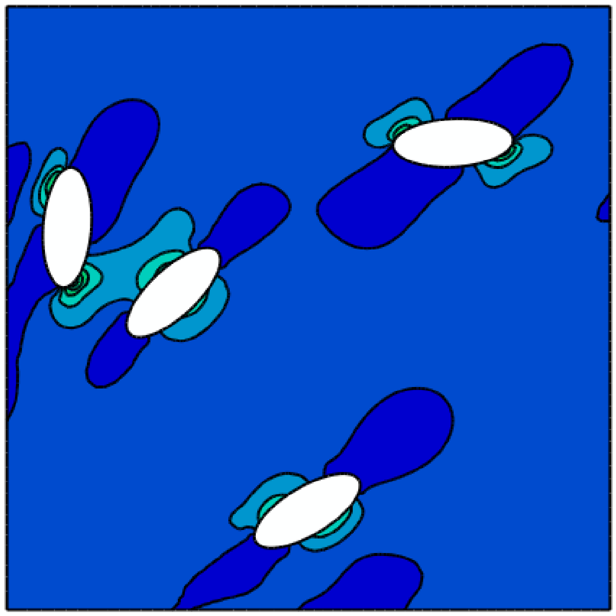

Figure 8. Maximum principal stress – test case with 4 holes.

The choice of mesh seed was felt to be important. The key objective here was not to get the best mesh for a given number of elements, but rather to ensure compatibility of result quality for results with different numbers of cracks. To this end, it was of vital importance that the mesh refinement of the elements on the boundaries of each of the ellipses was similar. To ensure that, mesh seeds were defined on each full and partial ellipse edge, with target mesh size of 0.04µm. For full ellipses, this would yield approximately 50 nodes around the circumference. The mesh seed applied to the edge of the domain was a little coarser, with size 0.1µm – corresponding to 50 nodes per edge.

The meshing was carried out automatically, using the "Medial Axis" option, selecting "Quad" elements only, and removing the tick from the "Minimize the mesh transition" option. The latter is important, as it forces the meshing algorithm to respect the mesh seed. In some cases, because of the need to transition meshes around awkwardly placed ellipses, the mesh in big patches of the domain was very much finer than the mesh around the ellipse edges. Each model contained between around five and eleven thousand elements.

An alternative approach would have been to use the "Advancing Front" algorithm. This generally produces more elements, and the mesh quality is perhaps more questionable as there is a far greater tendency for there to be nodes surrounded by 5 elements.

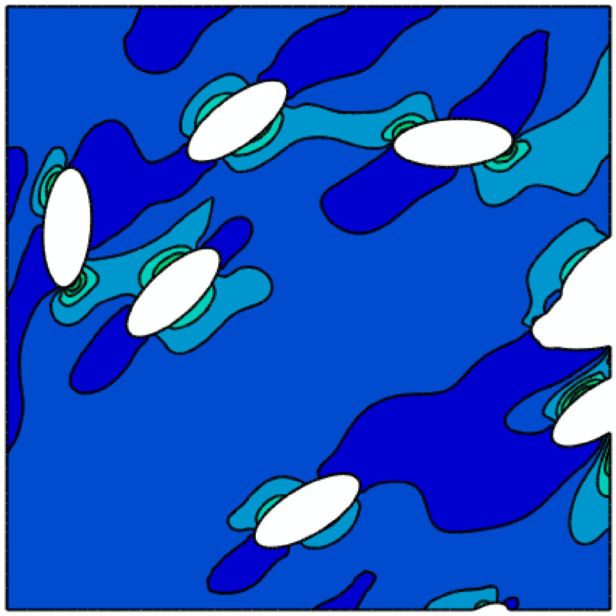

Figure 9. Maximum principal stress – test case with 8 holes.

4.3 Analysis

The analysis was performed in Abaqus implicit. The first analysis was for a domain with no hole, and for each subsequent analysis one ellipse was cut from the domain, in the sequence shown in table 1. On a fast laptop, each analysis took around 2 seconds.

5. Computational experiments – Results

The maximum principal stress results for four of the analyses are shown in figures 7 to 10. These give an indication of the influence of increasing crack density on the stress intensities around individual cracks. In some cases, the peak stress is reduced, as the crack is shielded by other cracks in the load path, but overall it leads to a smaller volume of the domain taking a larger proportion of the load. The overall trend is that the peak maximum principal stress increases with number of cracks in the domain.

The magnitudes of the minimum principal stresses were also observed to increase with number of cracks in the domain (figure 11). These stresses would be the maximum principal stresses if the loading direction were reversed. So, in a sense, this provides two data sets for the price of one!

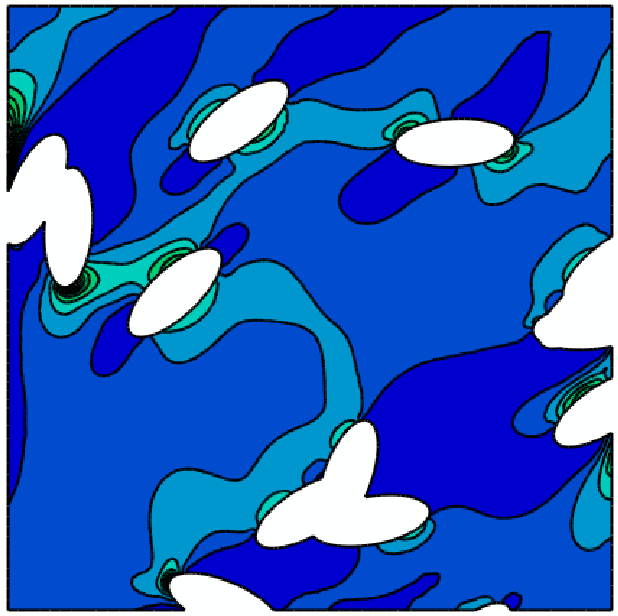

Figure 10. Maximum principal stress – test case with 12 holes.

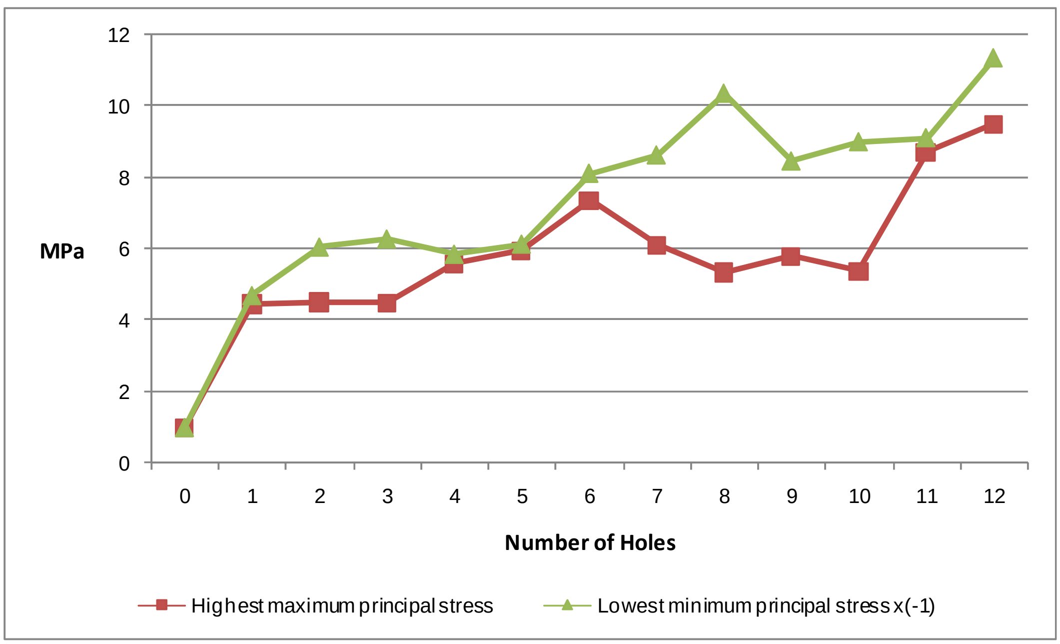

Figure 11. Predicted stress for increasing number of cracks.

Inspecting the relative magnitudes of the peak minimum and maximum principal stresses reveals something rather interesting: in this particular case study, the minimum principal stress magnitudes seem higher than those of the maximum principal stresses. This can be understood qualitatively in noting that most of the ellipses defined in the domain have an orientation between 0° and 90°. They are thus somewhat aligned to the overall shear field, and their shielding effect on each other is correspondingly reduced. With the load directions reversed, the ellipses tend to cross the load path lengthways, the shielding effect becomes higher, and the load path is pushed through a smaller volume of material. As a result, the stress intensity is higher at some of the most exposed ellipse ends.

6. Automation of analysis

Following these initial investigations, the next step is to create further RVEs models with other combinations of ellipses. Given that the above example becomes over-crowded with only a relatively small number of cracks, it was deemed appropriate to increase the domain size (side length 50µm) whilst maintaining the same size of ellipse. This should also answer concerns as to the quality of random location and orientation.

One issue already observed concerns the treatment of elliptical holes intersecting the domain boundary. In some cases, these lead to a considerable distortion of the boundary edge relative to what would be unacceptable for a RVE boundary assumption. Indeed, even cracks fully within the domain, but close to the edge, have such an effect. To avoid this problem, it was decided to maintain a margin around the domain that all ellipse centers must lie within. Given that the domain size is now defined to be much larger than the hole dimension, any edge effect should be less significant.

The modeling was then automated using Python scripts. Geometry creation presented no problems, however significant problems were encountered with automatic meshing. While for the small domain problems, the medial axis algorithm worked well, significant problems were encountered with the larger domain. The problem encountered was that although the mesh seed defined on the boundary of the domain was significantly coarser than that defined on the ellipse perimeters, the meshing algorithm was not adequately respecting the mesh seed on the elliptical holes.

Clearly, the main mesh requirement was a level of mesh refinement around each ellipse to capture the high stress gradients. In the far field, away from holes, the mesh should be much coarser in order to maintain manageable numbers of elements. The transition of mesh size, and the associated element shape quality, should be acceptable in all regions of the domain: this must be judged in terms of the smoothness of stress contour, and the absence of any spurious mesh related stress variations.

The obvious way forward was to introduce mesh partitions, in order to control the mesh topology. Ideally, the same partition would be used for every analysis, independently of the position and number of holes, to avoid complications in the scripting. This found to be totally inadequate giving poor element shape quality and led to regions of the mesh having unacceptably high numbers of elements. The best solution was found to partition depending on the hole locations. A script was written to create two partitions around each hole. The first partition was set to be elliptical, and aligned with the hole, with a view to creating a mesh of 3-5 concentric rings of elements. (In this case the partition had a semi-major axis length of 0.4µm and semi-minor of 0.2µm). An additional circular partition was also created, centered over the center of the hole, with a radius of 2µm. This was to ensure a well controlled mesh transition over the region of high stress gradient.

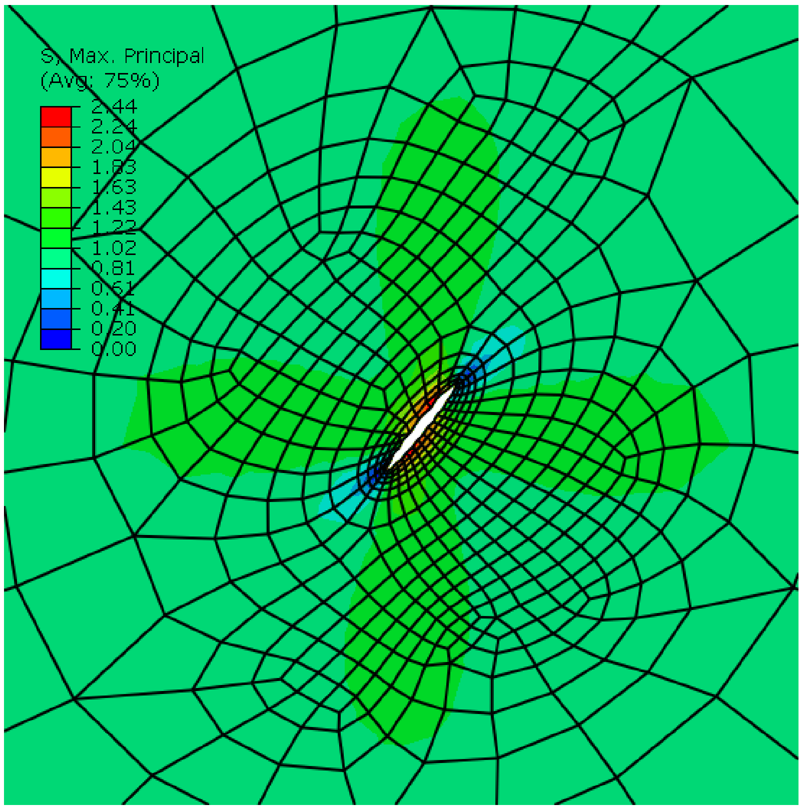

Figure 12. Partitioning for stable automatic meshing.

Figure 12 shows the mesh achieved using both types of partition, and the maximum principal stress achieved through this mesh. The inner elliptical partition is clearly visible as the largest of the concentric ellipses around the hole. The outer circular partition is identifiable as the outer ring of elements – slightly clipped to the right and bottom of the picture. It is clear that over 90% of the stress variation takes place well within this ring, and is captured adequately by this level of mesh refinement.

Using this partition method, in combination with mesh seeds, it is possible to achieve meshes comprising ~5000 elements. Analyses for such numbers of elements run in seconds, so multiple analyses should be achievable within hours or days.

7. Conclusions and further work

It has been established that increasing crack density can lead to increased stress intensity factor at the tips of some of these cracks. For a component subjected to loads leading to stresses in the resin near its strength limit, a high crack density would increase the tendency for propagation. The stress patterns seen in figures 7-10 indicate directions of potential crack path, joining neighboring cracks.

Unfortunately, following the difficulty with mesh generation, there has not yet been sufficient time to run the analyses for the large numbers of cracks in the large domain. This should enable a better quantification of the relationship between crack density and stress intensity increase, and will be presented at the conference.

The work so far addressed here has been concerned with stress intensities and crack initiation. The next major step is to consider crack growth, and chart the progress of cracks between the ellipses under cyclic loading. This will require the use of XFEM methods. The ultimate goal is to gain some understanding of the role of micro-cracks in the high-cycle fatigue strength of composites.

8. Acknowledgements

The author acknowledges the support of Rolls-Royce, and the financial support of the Royal Society through her Industry Fellowship.

9. References

1. Bailey, R. and Hicks, R. “Behaviour of perforated plates under plane stress”, Journal Mechanical Engineering Science, vol. 2, no. 2, pp. 143-165, 1960.
2. Gerlach, R., et al. “The interface between matrix pockets and fibre bundles under impact loading” submitted to Composites Science and Technology.
3. HEXCEL, “HexFlow® RTM 6” HEXCELRTM6.pdf click on RTM6 at http://www.hexcel.com/products/Matrix+Products/Other+FRM/RTM
4. Newman, E. I. “A method of estimating the total length of root in a sample”, The Journal of Applied Ecology, vol. 3, no. 1, pp139-145, 1966
5. Pilkey, W. D. “Peterson’s stress concentration factors”, 2nd Edition, Wiley-Interscience, New York, 1997.
6. Van Wagner, C. E. “Practical aspects of the line intersect method”, Petawawa National Forestry Institute, Canadian Forestry Service, Chalk River, Ontario, Canada, Information Report PI-X-12, 1982
7. Wilson, S.P., Taylor, D., “Reliability assessment from fatigue micro-crack data”, IEEE Transactions on Reliability, vol. 46, no. 2, pp 165-172, 1997